RSC Advances

PAPER

View Article Online
View Journal | View Issue

Cite this: *RSC Adv.*, 2015, **5**, 90235

The promotional role of Ce in Cu/ZSM-5 and *in situ* surface reaction for selective catalytic reduction of NO_x with NH_3†

Shuangshuang Lai, Dongmei Meng, Wangcheng Zhan,* Yun Guo, Yanglong Guo, Zhigang Zhang and Guanzhong Lu*

Cu/ZSM-5 and Ce doped Cu/ZSM-5 catalysts were prepared by the incipient-wetness-impregnation method, and the effect of Ce doping on the structure and the catalytic performance of the Cu/ZSM-5 catalyst was investigated in detail for the selective catalytic reduction (SCR) of NO with NH_3. The results showed that the addition of Ce can markedly broaden the operation temperature window of the Cu/ZSM-5 catalyst for NH_3-SCR and enhance its H_2O and SO_2 resistance. The presence of Ce promoted an enrichment of copper species (isolated Cu^{2+} ions and CuO nanoparticles) on the catalyst surface and the increase in the Lewis acid sites on the surface of the Cu/ZSM-5 catalyst, and strengthened the redox property of the Cu/ZSM-5 catalyst. As a result, Ce-doped Cu/ZSM-5 catalyst possessed the high adsorption ability of NH_3 and nitrite/nitrate, which is propitious to the increase in the reactivity of the Ce-doped Cu/ZSM-5 catalyst. *In situ* DRIFTS results indicated that the NH_3-SCR reaction on the Cu/ZSM-5 catalyst and Ce_1–Cu_4/ZSM-5 catalysts definitely followed Langmuir–Hinshelwood mechanisms, and bridged nitrates and bidentate nitrates were the active intermediate. However, Eley–Rideal mechanism can't be confirmed over the Cu/ZSM-5 and Ce_1–Cu_4/ZSM-5 catalysts.

Received 28th June 2015
Accepted 9th October 2015

DOI: 10.1039/c5ra12505g

www.rsc.org/advances

1. Introduction

Nitrogen oxides (NO_x) originated from various combustion processes are major air pollutants, which are very harmful to human health, due to the formation of photochemical smog, acid rain, ozone depletion and greenhouse effects. The selective catalytic reduction of NO_x with ammonia (NH_3-SCR) in the presence of excess oxygen has been considered as one of the best available approaches to control the emission of NO_x produced from the stationary sources and the diesel vehicle. V_2O_5–$WO_3(MoO_3)/TiO_2$ behaves the high activity and selectivity of NH_3-SCR and has been the most widely used in industry.[1] However, there are still some inevitable problems, such as the narrow working temperature window (300–400 °C), the toxicity of vanadium species,[2] and the low N_2 selectivity at high temperatures.[3] Therefore, it is necessary to develop vanadium-free catalysts with high SCR activity.

In recent years, the zeolite-based catalysts are considered to be a practical solution for reducing the exhaust pollutants from diesel engines, and exhibit the high activities and good stability at high temperatures,[4,5] especially the Cu/ZSM-5 catalyst due to its superior SCR activity and N_2 selectivity in a wide temperature range.[6] However, previous researches indicated that the Cu/ZSM-5 catalyst did not possess a high SCR activity at high temperature.[7] With respect to monometallic copper loaded catalysts, it is difficult to enhance its SCR activity simply by increasing the copper content in the Cu/ZSM-5 catalyst. This is because a high content of copper inevitably leads to agglomeration of the copper species and formation of large copper oxide particles,[8] which would enhance the oxidation of NH_3 and narrow the temperature window. It has been determined that the optimal content of copper in the Cu/ZSM-5 catalyst is within 3–4 wt%.[9]

Ceria has been studied extensively as an oxygen reservoir, which can store and release oxygen by the redox cycle between Ce^{3+} and Ce^{4+} under oxidizing and reducing conditions.[10–12] Many Ce doped catalysts were studied extensively and used in the various reactions, including CeO_2–MnO_x,[10,13] $CeWO_x$,[14] Ce–Mn/ZSM-5,[11] and Ce–Cu/ZSM-5.[15,16] Recently, it was reported that Ce–Cu/ZSM-5 catalyst was used for NH_3-SCR reaction. Pang *et al.*[17] reported that adding Ce into Cu/ZSM-5 monolithic catalyst could obviously improve its activity and hydrothermal stability by stabilizing the dispersion of CuO and suppressing the formation of bulk-type CuO crystallites during hydrothermal treatment. Dou *et al.*[18] also

---

Key Laboratories for Advanced Materials, Research Institute of Industrial Catalysis, East China University of Science and Technology, 130 Meilong Road, Shanghai 200237, China. E-mail: gzhlu@ecust.edu.cn; zhanwc@ecust.edu.cn; Fax: +86-21-64252923

† Electronic supplementary information (ESI) available. See DOI: 10.1039/c5ra12505g

confirmed that Ce doping improved the redox properties of the Cu–Ce/ZSM-5 catalyst, due to the higher valence of copper and mobility of lattice oxygen than those of Cu/ZSM-5 catalyst. But little attention has been paid to the effect of Ce doping on the acid sites, surface species and adsorption property of Ce–Cu/ZSM-5 catalysts. And the surface reaction mechanism over the Ce–Cu/ZSM-5 catalyst for the NH_3-SCR reaction and the role of Ce on the catalytic cycle has not been investigated.

Herein, we try to solve two problems for Ce doped Cu/ZSM-5 catalysts, the promotional role of Ce and the surface reaction mechanism over the Ce–Cu/ZSM-5 catalyst for the NH_3-SCR reaction, including the effect of Ce doping on the SO_2 resistance and water resistance. These research results will certainly be useful for the further development of the zeolite catalysts for the NH_3-SCR reaction.

2. Experimental

2.1 Preparation of catalysts

A series of Ce_x–Cu_4/ZSM-5 catalysts with copper content of 4 wt% and variable content of cerium were prepared by an improved incipient-wetness-impregnation method. H–ZSM-5 with Si/Al atomic ratio of 18 was supplied by Nankai University, Tianjin, China. In a typical process, the required amount of an aqueous solution of $Cu(NO_3)_2\cdot 3H_2O$ and $Ce(NO_3)_3\cdot 6H_2O$ was slowly dropped into the support under vigorous stirring at room temperature, and then ultrasonically treated for 1 h. The content of copper in the catalysts was maintained at 4 wt%, and the content of cerium was varied. The solid was dried at 120 °C for 12 h and calcined in air at 550 °C for 4 h. The final catalysts were labeled as Ce_x–Cu_4/ZSM-5 (x denotes the weight ratio of Ce/H–ZSM-5, x = 0.5, 1, 2 wt%).

The Cu_4/ZSM-5 catalyst was also prepared with the same procedure as Ce_x–Cu_4/ZSM-5, but no $Ce(NO_3)_3\cdot 6H_2O$ was added in the synthesis solution.

2.2 Catalyst characterization

The XRD patterns were recorded on a Brook/D8 diffractometer with CuKα Radiation ($\lambda = 0.154056$ nm) in the 2θ range of 5–60°. The morphologies of the catalysts were investigated by field emission scanning electron microscopy (FE-SEM) on a Hitachi S-4800 instrument operated at the beam energy of 15 kV. The N_2 adsorption–desorption isotherms were measured on a Quantachrome NOVA1200 surface area at −196 °C. Prior to the measurements, all samples were degassed at 180 °C until a stable vacuum of *ca.* 5 mTorr was reached. The surface areas of the samples were calculated by Brunauer–Emmett–Teller (BET) method. The pore size distribution were calculated from the desorption branch using the Barrett–Joyner–Halenda (BJH) method. The XPS spectra were recorded on a Thermo ESCALAB 250 spectrometer with a monochromatized AlKα X-ray source (1486.6 eV) and a passing energy of 25 eV. C1s (binding energy 284.6 eV) of adventitious carbon was used as the reference.

Py-IR spectra of samples were analyzed by a Nicolet 5700 FT-IR spectrometer. The samples (13 mg) was heated at 400 °C under vacuum for 2 h, and cooled to 200 °C when pyridine was chemisorbed for 10 min. After this step, the sample was evacuated and analyzed by FTIR.

Temperature-programmed desorption of NH_3 (NH_3-TPD) was carried out on a PX200 apparatus (Tianjin Pengxiang Technology Ltd. China) with a thermal conductivity detector (TCD). 50 mg of the sample was filled into the quartz reactor and pretreated at 500 °C in a flow of N_2 (50 mL min^{-1}) for 1 h. After being cooled down to room temperature, the sample was exposed to a flow of 10% NH_3/N_2 (50 mL min^{-1}) for 0.5 h. Then the sample was flushed by N_2 (50 mL min^{-1}) for 1 h and NH_3-TPD was carried out by heating the sample in N_2 (50 mL min^{-1}) from room temperature to 500 °C at 10 °C min^{-1}.

NO-TPD was carried out on the custom-made equipment with a NO_x analyzer (Thermo Fisher Model 42i-HL NO–NO_x-chemiluminescence analyzer) as detector. The sample was pretreated in Ar (450 mL min^{-1}) at 450 °C for 1 h and cooled down to room temperature. Then the sample was exposed to a flow of 500 ppm NO/Ar (300 mL min^{-1}) for 1 h to reach saturated adsorption of NO on the sample, followed by Ar (300 mL min^{-1}) purging for 1 h. Finally, NO-TPD was carried out by heating the sample in Ar (300 mL min^{-1}) from room temperature to 450 °C at 10 °C min^{-1}.

Temperature-programmed reduction with H_2 (H_2-TPR) was performed in a conventional flow apparatus. 100 mg of the sample was used. A flow of 5% H_2/N_2 (40 mL min^{-1}) was passed through the catalyst bed at 10 °C min^{-1} from 30 to 600 °C. The consumption of hydrogen was monitored by a thermal conductivity detector (TCD).

The *in situ* DRIFT measurements were performed on a Nicolet 6700 FT-IR spectrometer with a MCT detector. The sample was pretreated at 500 °C in Ar for 1 h, and then cooled to 150 °C in Ar. The background spectra were recorded at the different temperatures during the cooling, and background was subtracted from sample spectra accordingly.

2.3 Catalytic activity testing

The catalytic activities of the Ce_x–Cu_4/ZSM-5 catalysts for NH_3-SCR in excess oxygen were investigated in a fixed-bed quartz reactor (Φ 6 mm × 300 mm). 200 mg of the catalyst (20–40 mesh) was used. The reactant gas was composed of 500 ppm NO, 500 ppm NH_3, 5 vol% O_2, 2 vol% H_2O (when used), 50 ppm SO_2 (when used) and balanced Ar. The gas hourly space velocity (GHSV) was 55 000 h^{-1}. The concentrations of NO and NO_2 remained in the product were analysed by a Thermo Fisher NO–NO_x-chemiluminescence analyzer. To avoid modest errors caused by the oxidation of ammonia in the converter of NO/NO_x analyzer, an ammonia trap containing phosphoric acid solution was installed prior to the chemiluminescence detector. NO_x conversion $X(NO_x)$ was calculated as follows:

$$X(\mathrm{NO}_x) = \frac{[\mathrm{NO}_x]_{\mathrm{in}} - [\mathrm{NO}_x]_{\mathrm{out}}}{[\mathrm{NO}_x]_{\mathrm{in}}} \times 100\%$$

3. Results and discussion

3.1 Catalytic performance for NH_3-SCR activity

The catalytic activities of the Cu_4/ZSM-5 and Ce_x–Cu_4/ZSM-5 catalysts for the NH_3-SCR reaction are shown in Fig. 1. The H–ZSM-5 catalyst exhibited a very low activity, over which the maximum NO_x conversion is only 80% at 425 °C. The Cu_4/ZSM-5 catalyst has a high catalytic activity, and the NO_x conversion of above 90% was obtained at 195–435 °C.

When cerium was added to Cu_4/ZSM-5, the catalytic activity of Cu_4/ZSM-5 toward NH_3-SCR reaction was significantly improved, especially at the high temperature. For example, when the Ce_1–Cu_4/ZSM-5 catalyst was used, the temperature window of more than 90% NO_x conversion was 185–470 °C; while for the Ce_2–Cu_4/ZSM-5 and $Ce_{0.5}$–Cu_4/ZSM-5 catalysts, their window were 180–460 °C and 175–450 °C, respectively. The results clearly demonstrate that comparing with the operation window of Cu_4/ZSM-5 catalyst, adding an appropriate amount of Ce in this catalyst can broaden the operation window about 45 °C. Furthermore, the amount of Ce obviously affects the NH_3-SCR activity of the Ce_x–Cu_4/ZSM-5 catalyst at the high temperature, while this influence is faint at the low temperature.

On the other hand, both the Cu_4/ZSM-5 and Ce_1–Cu_4/ZSM-5 catalysts behaved the high stability after the NH_3-SCR reaction. As shown in Fig. S1,† the NH_3-SCR activities of the Cu_4/ZSM-5 and Ce_1–Cu_4/ZSM-5 catalysts on the second run are almost the same as those on the first run.

3.2 Physicochemical properties of catalysts

Fig. 2 shows the XRD patterns of H–ZSM-5, Cu_4/ZSM-5 and Ce_x–Cu_4/ZSM-5 catalysts. All the samples exhibit the typical diffraction peaks of ZSM-5 zeolite at $2\theta = 7.9°$, 8.8°, 23.1° and 23.8°, which represent the (011), (020), (051) and (033) planes, respectively.[19] Comparing with the XRD spectrum of H–ZSM-5, the XRD spectra of Cu_4/ZSM-5 and Ce_x–Cu_4/ZSM-5 catalysts were changed inconspicuously, which indicates that the structure of zeolite support remains intact after adding Cu and Ce. On the other hand, the diffraction peaks of CuO are not detected for all catalysts, showing that the copper species are well dispersed on the surface of the ZSM-5 support, or aggregated crystallites are too small to be detected by XRD. Similarly, the diffraction peaks of CeO_2 are not also detected for the Ce_x–Cu_4/ZSM-5 catalysts with low Ce content. However, with increasing the Ce content to 2.0 wt%, the very weak diffraction peak of CeO_2 can be observed ($2\theta = 28.2°$) for the Ce_2–Cu_4/ZSM-5 catalyst, indicating the formation of CeO_2 crystallites on the surface of the Ce_2–Cu_4/ZSM-5 catalyst.

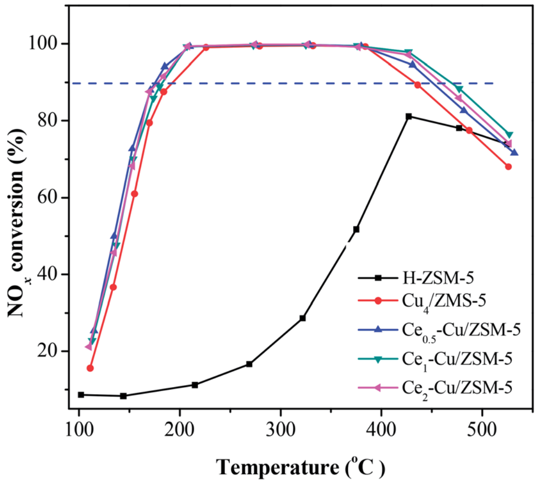

Fig. 1 NO_x conversion as a function of the reaction temperature over Cu/ZSM-5 and Ce_x–Cu_4/ZSM-5 catalysts for the NH_3-SCR reaction. (Reaction conditions: 0.2 g catalyst, the reactant gas of 500 ppm NO/500 ppm NH_3/5% O_2/Ar balanced, GHSV = 55 000 h^{-1}).

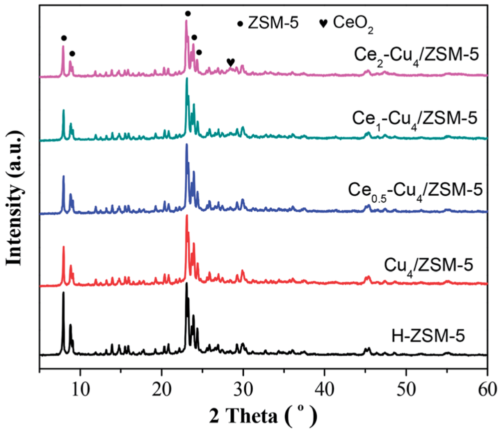

Fig. 2 Wide-angle XRD patterns of pure H–ZSM-5, Cu_4/ZSM-5 and Ce_x–Cu_4/ZSM-5 catalysts.

Fig. 3 shows the SEM images of H–ZSM-5, Cu_4/ZSM-5 and Ce_1–Cu_4/ZSM-5 catalysts. The results show that, H–ZSM-5 exhibits the schistose and irregular morphology, and after the addition of Cu and Ce, the morphologies of Cu_4/ZSM-5 and Ce_x–Cu_4/ZSM-5 catalysts are virtually unchanged. The BET surface area, average pore diameter and micro-pore volume are listed in Table 1. It can be seen that adding Cu leads to the decrease in

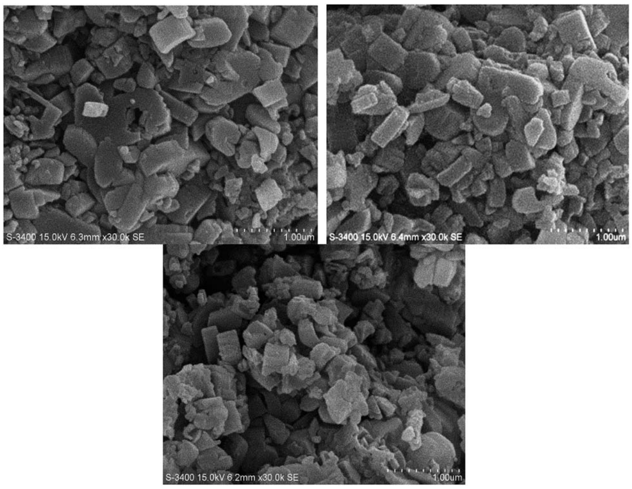

Fig. 3 SEM images of pure H–ZSM-5 (top left), Cu_4/ZSM-5 (top right) and Ce_1–Cu_4/ZSM-5 (bottom).

Table 1 BET surface area (S_{BET}) and surface atom concentrations of the Cu_4/ZSM-5 and Ce_1–Cu_4/ZSM-5 catalysts derived from XPS data

					Surface composition (at%)		
Sample	S_{BET} ($m^2\ g^{-1}$)	Average pore diameter (nm)	Micro-pore volume ($cm^3\ g^{-1}$)	Isolated Cu^{2+}/CuO[a]	Cu (isolated Cu^{2+}/CuO)[b]	Ce	O
H–ZSM-5	333	2.1	0.14	—	—	—	—
Cu_4/ZSM-5	280	1.6	0.12	0.239	1.59 (0.31/1.28)	—	63.2
Ce_1–Cu_4/ZSM-5	268	1.6	0.12	0.247	1.97 (0.39/1.58)	0.25	62.8

[a] The peak area ratio (m) of M (isolated Cu^{2+} ions)/M (CuO crystallites) in XPS spectrum. [b] "Isolated Cu^{2+}" was calculated by Cu (at%) × (m/(1 + m)) and "CuO" was calculated by Cu (at%)/(1 + m).

BET surface area, average pore diameter and micro-pore volume, which can be attributed to the fact that copper species cover the external surface of H–ZSM-5, blocking many zeolite channels. After the addition of Ce into the Cu_4/ZSM-5 catalyst, BET surface area was decreased slightly, while average pore diameter and micro-pore volume remained unchanged.

Fig. 4 shows XPS Cu2p spectra of Cu_4/ZSM-5 and Ce_1–Cu_4/ZSM-5 catalysts. The Cu_4/ZSM-5 catalyst has two main peaks at BE = 933.6 eV and 953.0 eV in its XPS Cu2p spectra, which are attributed to Cu2p3/2 and Cu2p1/2, respectively. The Cu2p3/2 peaks can be deconvoluted to two peaks, and the peaks at 933.4 eV represent the agglomerated CuO nanoparticles on the surface of catalysts, and the one at BE = 935.2 eV is attributed to isolated Cu^{2+} ion coordinated to superficial oxygen atoms of zeolite.[18,20] Since the diffraction peaks of CuO species could not be observed in the XRD spectra, these CuO crystallites' size should be lower than 3 nm.

Table 1 shows the surface atom concentrations of Cu_4/ZSM-5 and Ce_1–Cu_4/ZSM-5 catalysts. It can be seen that surface Cu amount increases with the addition of Ce in the Cu_4/ZSM-5 catalyst, indicating that the presence of Ce can help to the enrichment of Cu on the Cu_4/ZSM-5 surface. According to the peak area ratio of (isolated Cu^{2+} ions)/(CuO crystallites) in XPS spectra, the amounts of isolated Cu^{2+} ions and CuO crystallites on the surface of Cu_4/ZSM-5 and Ce_1–Cu_4/ZSM-5 catalysts were calculated (Table 1). The results show that CuO crystallites are predominant on the surface of both Cu_4/ZSM-5 and Ce_1–Cu_4/ZSM-5 catalysts with a high Cu content, which is consistent with the reported results.[20] Furthermore, the surface concentrations of isolated Cu^{2+} ions and CuO crystallites over the Ce_1–Cu_4/ZSM-5 catalyst are higher than that over the Cu_4/ZSM-5 catalyst, because of the increase of the surface Cu atoms after Ce addition in the Cu_4/ZSM-5 catalyst.

Wang *et al.*[21] thought both CuO nanoparticles and isolated Cu^{2+} ion in Cu/SAPO-34 were active sites for the NH_3-SCR reaction. Furthermore, it is revealed that the CuO nanoparticles catalyzes the oxidation of NO to NO_2, and this favors the reduction of NO at lower temperature due to the facilitation of the "fast SCR" process, while isolated Cu^{2+} ions help to the high NO conversion at high temperature. Therefore, when adding Ce in the Cu_4/ZSM-5 catalyst, the increase in the surface concentrations of both isolated Cu^{2+} ions and CuO nanoparticles can improve the activity of the Cu_4/ZSM-5 catalyst.

Fig. 5 shows the UV-Vis absorption spectra of H-ZSM-5, Cu_4/ZSM-5 and Ce_1–Cu_4/ZSM-5 catalysts. H-ZSM-5 exhibits the adsorption bands at about 210 and 280 nm. For Cu_4/ZSM-5, a band at 258 nm and a broad band centered at 750 nm between 550 and 800 nm appeared. The former can be assigned to O → Cu transitions of isolated Cu^{2+} ions in coordination with lattice oxygen, and the latter can be assigned to d–d transitions

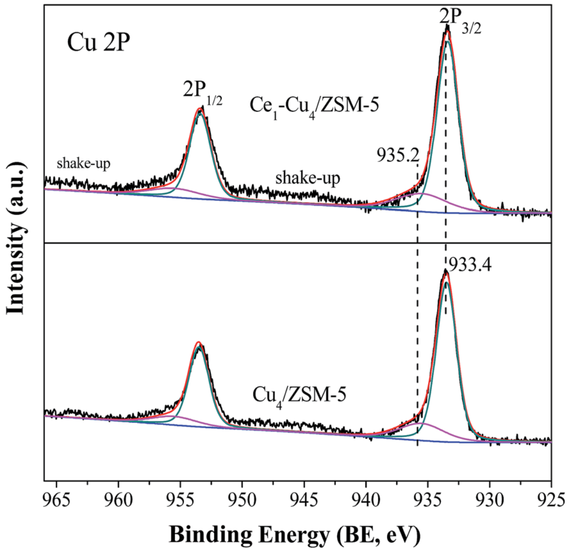

Fig. 4 XPS Cu2p spectra of Cu_4/ZSM-5 and Ce_1–Cu_4/ZSM-5 catalysts.

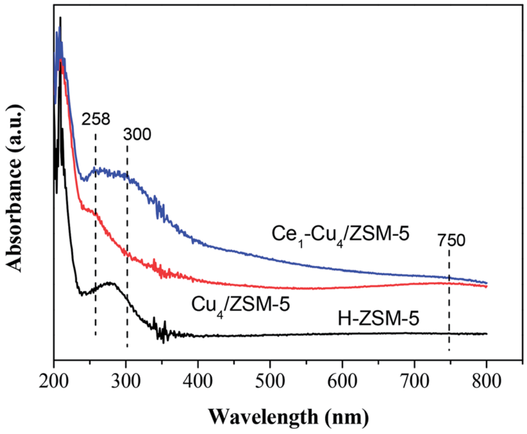

Fig. 5 UV-Vis spectra of H-ZSM-5, Cu_4/ZSM-5 and Ce_1–Cu_4/ZSM-5 catalysts.

of Cu^{2+} ions in a octahedrically coordinated environment due to dispersed CuO crystallites on the catalyst surface.[22–24] When cerium was added to Cu_4/ZSM-5, a broad band centered at 300 nm appeared, which can be attributed to well-dispersed Ce species on the surface of catalyst (presumably in a tetra-coordinated environment), which is confirmed by the XRD results.[25] Meanwhile, the intensity of 258 nm band was increased compared with that in UV-Vis spectra of Cu_4/ZSM-5 catalyst, indicating the increase in the amount of isolated Cu^{2+} ions, which is consistent with the XPS results. On the contrary, it is difficult to quantify CuO crystallites on the catalyst surface because two bands centered at 300 and 750 nm overlap complexity.

3.3 Temperature-programmed desorption

Fig. 6 shows NH_3-TPD profiles of the H–ZSM-5, Cu_4/ZSM-5 and Ce_1–Cu_4/ZSM-5 catalysts in the temperature range of 100–500 °C. Two desorption peaks at 200 and 410 °C can be observed for the H–ZSM-5 catalyst. The desorption peak at 200 °C is assigned to physisorbed NH_3 or ammonium species, and the desorption peak at 410 °C is assigned to NH_3 absorbed at the strong acid sites.[26]

After adding copper and cerium, the NH_3-TPD profiles have been obviously changed. The desorption peak at 410 °C radically decreased for the Cu_4/ZSM-5 and Ce_1–Cu_4/ZSM-5 catalysts. On the contrary, a shoulder peak at 306 °C presented for the Cu_4/ZSM-5 and Ce_1–Cu_4/ZSM-5 catalysts. The reasons for this phenomena were because part of Brønsted acid protons were substituted by metal ion and strong Lewis acid sites were produced originating from metal oxide nanoparticles when adding Cu and/or Ce into the H–ZSM-5 catalyst.[27,28] Compared with the Cu_4/ZSM-5 catalyst, the peak area at 306 °C is slightly larger for the Ce_1–Cu_4/ZSM-5 catalyst, even if the specific surface area was considered, because the BET surface area ($268\ m^2\ g^{-1}$) of the former is less than that ($280\ m^2\ g^{-1}$) of the latter, indicating that the Ce_1–Cu_4/ZSM-5 catalyst possessed the more strong acid sites than that on the Cu_4/ZSM-5 catalyst.

Fig. 7 shows IR spectra of adsorbed pyridine on H–ZSM-5, Cu_4/ZSM-5 and Ce_1–Cu_4/ZSM-5 catalysts. The absorption bands at 1450 cm^{-1} and 1545 cm^{-1} are assigned to Lewis acid sites and Brønsted acid sites respectively, while the absorption band at 1490 cm^{-1} is assigned to both of them. The concentration of the Lewis acid sites (LA) and Brønsted acid sites (BA) were calculated from the intensity of the absorption bands at 1450 cm^{-1} and 1545 cm^{-1}, and the results are shown in Table 2. It can be seen that the H–ZSM-5 catalyst mainly exhibited Brønsted acid sites. After adding copper, the amount of Brønsted acid sites markedly decreased due to the ion exchange during the preparation step. On the contrary, the amount of Lewis acid sites increased largely because of the presence of Cu^{2+} ions on the surface. Furthermore, compared with the H–ZSM-5 catalyst, the Cu_4/ZSM-5 catalyst possessed the higher amount of total acid sites. When adding cerium into the Cu_4/ZSM-5 catalyst, the amounts of both the Lewis acid sites and Brønsted acid sites were increased, leading to the higher amount of total acid sites, which is in accordance with the NH_3-TPD results. It has been proved that Brønsted acid sites may not be required for activating ammonia, while Lewis acid sites plays an important role on the NH_3-SCR process catalyzed by the zeolite catalyst.[29] Therefore, the more Lewis acid sites over the Ce_1–Cu_4/ZSM-5 catalyst might make the higher NH_3-SCR activity of Ce_1–Cu_4/ZSM-5 than the Cu_4/ZSM-5 catalyst.

The NO-TPD profiles of the catalysts are also shown in Fig. 8. Two obvious desorption peaks centered at 120 and 400 °C presented in the NO-TPD profile of the Cu_4/ZSM-5 catalyst. The desorption peak at 120 °C can be attributed to physisorbed NO_x, and the desorption peak at 400 °C is due to the decomposition of nitrite and nitrate species with higher thermal stability.[30] After adding Ce in the Cu_4/ZSM-5 catalyst, the desorption peak area at 400 °C increased remarkably, indicating that the addition of Ce can enhance the adsorption of nitrite and nitrate species on the surface of the Cu_4/ZSM-5 catalyst. In addition, the presence of Ce in this catalyst also improves the adsorption

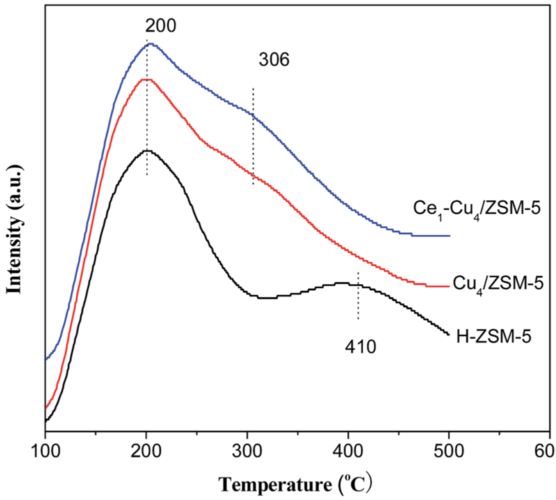

Fig. 6 NH_3-TPD profiles of H–ZSM-5, Cu_4/ZSM-5 and Ce_1–Cu_4/ZSM-5 catalysts.

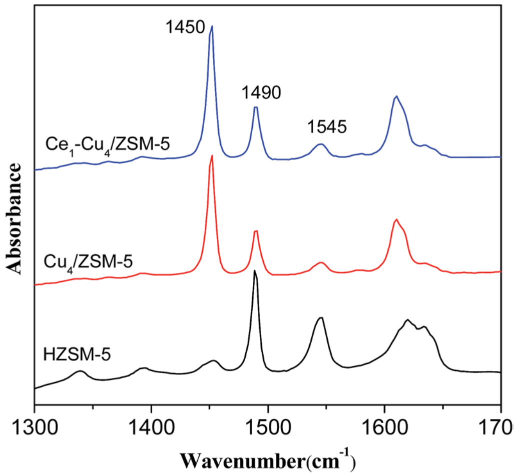

Fig. 7 IR spectra of adsorbed pyridine on H–ZSM-5, Cu_4/ZSM-5 and Ce_1–Cu_4/ZSM-5 catalysts.

Table 2 Acidity of the H–ZSM-5, Cu_4/ZSM-5 and Ce_1–Cu_4/ZSM-5 catalysts derived from IR spectra of adsorbed pyridine

Sample	LA[a] (μmol mg^{-1})	BA[b] (μmol mg^{-1})	Total of acid sites (μmol mg^{-1})
H–ZSM-5	0.41	2.10	2.52
Cu_4/ZSM-5	2.75	0.42	3.17
Ce_1–Cu_4/ZSM-5	3.08	0.54	3.62

[a] The Lewis acid sites. [b] The Brønsted acid sites.

capacity and ability for NO at low temperature. As a result, more nitrite and nitrate species on the Ce_1–Cu_4/ZSM-5 catalyst surface can participate the SCR reaction than that on the surface of the Cu_4/ZSM-5 catalyst, and the Ce doped catalyst can adsorb NO at lower temperature, resulting in the enhancement of the catalytic activity and the extension of the operation temperature window of the Ce_1–Cu_4/ZSM-5 catalyst.

3.4 H_2-TPR

Fig. 9 shows H_2-TPR profiles of H–ZSM-5, Cu_4/ZSM-5 and Ce_1–Cu_4/ZSM-5 catalysts. The H–ZSM-5 catalyst does not exhibit any reduction peaks. There are three reduction peaks at 213, 245 and 330 °C in the TPR profile of the Cu_4/ZSM-5 catalyst. The reduction peak at 213 °C is attributed to the reduction of CuO nanoparticles dispersed on the ZSM-5 surface to Cu^0, and the reduction peaks at 245 and 330 °C are assigned to the reduction of isolated Cu^{2+} to Cu^0 through two steps.[31] The reduction $Cu^{2+} \rightarrow Cu^+$ can occur at lower temperature, and the reduction $Cu^+ \rightarrow Cu^0$ only can carry out at higher temperature. For the Ce_1–Cu_4/ZSM-5 catalyst, there are also three reduction peaks, the peak at 330 °C shifted to a higher temperature of 350 °C, and the reduction peak area at 213 °C was markedly increased comparing with the Cu_4/ZSM-5 catalyst, due to the high surface concentrations of CuO nanoparticles (Table 1). The results above show that adding Ce in the Cu_4/ZSM-5 catalyst can enhance its reducibility.

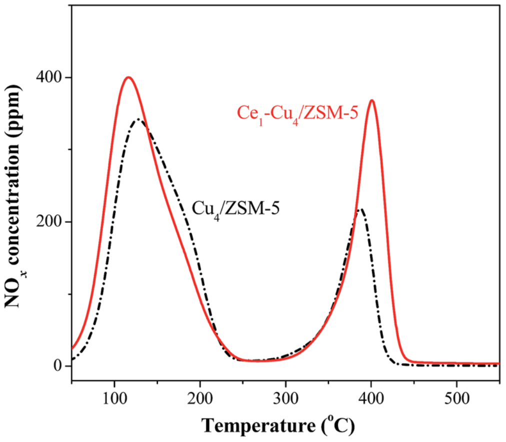

Fig. 8 NO-TPD profiles of the Cu_4/ZSM-5 and Ce_1–Cu_4/ZSM-5 catalysts.

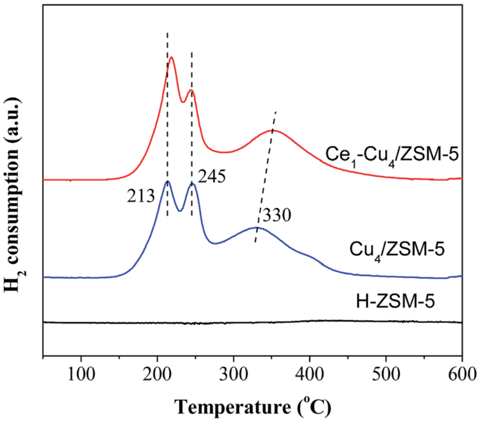

Fig. 9 H_2-TPR profiles of H–ZSM-5, Cu_4/ZSM-5 and Ce_1–Cu_4/ZSM-5 catalysts.

3.5 NO oxidation

It is well known that the improvement of NO oxidation to NO_2 over SCR catalysts can significantly promote its low temperature activity, due to the occurrence of the "fast SCR", $NO + NO_2 + 2NH_3 \rightarrow 2N_2 + 3H_2O$.[32] Therefore, the effect of adding Ce on the catalytic activity of the Cu_4/ZSM-5 catalyst for NO oxidation has been investigated. As shown in Fig. 10, for the NO oxidation at <400 °C, the activity of the Ce_1–Cu_4/ZSM-5 catalyst is slightly higher than that of the Cu_4/ZSM-5 catalyst, due to the higher reducibility of the Ce_1–Cu_4/ZSM-5 catalyst. At the high temperature, there is no difference of the catalytic activity of both catalysts for NO oxidation because of the equilibrium conversion.

3.6 *In situ* DRIFT spectroscopy

3.6.1 Adsorption of NH_3 followed by introduction of NO + O_2.

Prior to NH_3 adsorption, the catalyst was pretreated at 500 °C in the Ar flow of 50 mL min^{-1} for 1 h and cooled to 150 °C, and then the catalyst was exposed to the gas of 500 ppm NH_3/Ar

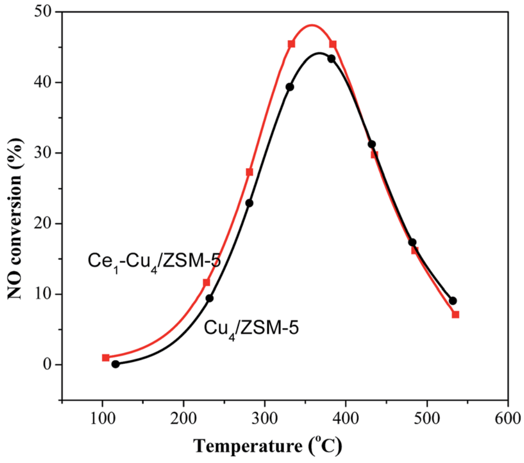

Fig. 10 NO conversion in separate NO oxidation reaction over the Cu_4/ZSM-5 and Ce_1–Cu_4/ZSM-5 catalysts. (Reaction conditions: 500 ppm NO + 5 vol% O_2/Ar balanced, total flow rate 300 mL min^{-1}).

(50 mL min^{-1}) at 150 °C, while *in situ* DRIFT spectra of the Cu_4/ZSM-5 (or Ce–Cu_4/ZSM-5) catalyst were taken for different times, and the DRIFT spectra of NH_3 adsorbed on catalysts are presented in Fig. 11.

The bands at 1159 and 1255, 1604 cm^{-1} are assigned to coordinated NH_3 adsorbed on Lewis acid sites, the bands at 1469 and 1734 cm^{-1} are assigned to NH^{4+} ions located on Brønsted acid sites.[19,33–36] And the band at 1519 cm^{-1} might be attributed to amide (–NH_2) species.[19,37] With an increase in the exposure time, the intensities of all bands are obviously increased, indicating the increase in the amount of adsorbed NH_3 species. After adding Ce in the Cu_4/ZSM-5 catalyst, its *in situ* DRIFT spectra are similar to that of the Cu_4/ZSM-5 catalyst. The coordinated NH_3 adsorbed on Lewis acid sites (bands at 1158, 1253 and 1606 cm^{-1}), and NH^{4+} ions located on Brønsted acid sites (bands at 1469 and 1734 cm^{-1}) are also presented, and their intensities are increased obviously with the increase in the exposure time of NH_3. As shown in Fig. 11, Lewis acid sites on the two catalysts are dominant to adsorb or activate NH_3 compared with Brønsted acid sites, because most of Brønsted acid sites have been substituted by Ce or Cu ions.[38]

After the experiments of Fig. 11 were finished, the catalyst was purged with Ar (50 mL min^{-1}) for 1 h, and then was exposed to 500 ppm NO + 5 vol% O_2/Ar (50 mL min^{-1}). *In situ* DRIFT spectra of the catalyst were taken for different times and are presented in Fig. 12.

As shown in Fig. 12A, when NO + O_2 is exposed to NH_3-pretreated Cu_4/ZSM-5 catalyst, the intensities of the bands at 1159, 1255, 1604, 1519 and 1734 cm^{-1} decreased gradually with the increase in the exposure time of NO + O_2, which indicates that both NH_3 species adsorbed on Lewis acid sites and NH_4^+ ions located on Brønsted acid sites are involved in the NH_3-SCR reaction. At the same time, many new bands at 1678 and 1569 cm^{-1} ascribed to nitrates species appeared and increased with the increase of the exposure time in NO + O_2. After adding Ce, the bands assigned to adsorbed NH_3 species decreased more quickly on the Ce_1–Cu_4/ZSM-5 catalyst with the increase in the exposure time of NO + O_2 (Fig. 12B), indicating the higher SCR activity compared with the Cu_4/ZSM-5 catalyst.

3.6.2 Adsorption of NO + O_2 followed by introduction of NH_3.

Prior to the adsorption of NO + O_2, the catalyst was pretreated at 500 °C in Ar (50 mL min^{-1}) for 1 h. After the catalyst was cooled down to 150 °C, Ar gas was replaced by the mixed gas of 500 ppm NO + 5 vol% O_2/Ar (50 mL min^{-1}), and *in situ* DRIFT spectra of the Cu_4/ZSM-5 and Ce_1–Cu_4/ZSM-5 catalysts were taken for different times, and their results are shown in Fig. 13.

As shown in Fig. 13A, there are three strong bands at 1679, 1628 and 1568 cm^{-1} in the DRIFT spectra of the Cu_4/ZSM-5 catalyst. The bands at 1628 and 1568 cm^{-1} are assigned to bridged and bidentate nitrates respectively,[39–42] and the band at 1679 cm^{-1} is attributed to ionic nitrite species.[43,44] These bands were increased with the exposure time. Besides, there are still three bands with low intensity at 1438, 1303 and 1200 cm^{-1} in the DRIFT spectra of the Cu_4/ZSM-5 catalyst. These bands are assigned to nitrite species.[42,44,45]

Compared with the *in situ* DRIFT spectra of the Cu_4/ZSM-5 catalyst, the strong absorption bands at 1679, 1626 and 1569 cm^{-1} are also shown in the *in situ* DRIFT spectra of the Ce_1–Cu_4/ZSM-5 catalyst (Fig. 13B), but the intensity of the absorption band at 1679 cm^{-1} corresponding to ionic nitrite species is much lower than those at 1626 and 1569 cm^{-1}. This is because that the higher oxidation of the Ce_1–Cu_4/ZSM-5 catalyst (as shown in H_2-TPR results) can easily oxidize ionic nitrite species to nitrates, resulting in the reduction in the ionic nitrite species on the Ce_1–Cu_4/ZSM-5 catalyst surface. At the same time, the intensities of the bands at 1438 and 1303 cm^{-1} are much low, and the band at 1200 cm^{-1} assigned to bridged nitrite has even disappeared. Since nitrates are the active species for the SCR reaction, the highly catalytic activity of the Ce_1–Cu_4/ZSM-5 catalyst for the oxidation of nitrite to nitrate is favorable for the better SCR activity.

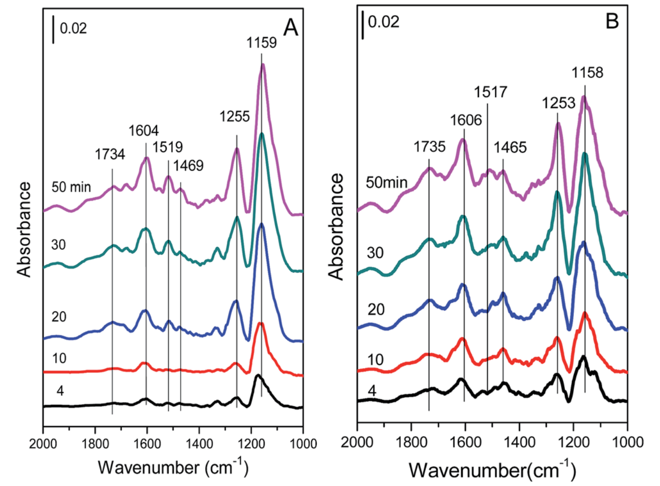

Fig. 11 *In situ* DRIFT spectra of (A) Cu_4/ZSM-5 and (B) Ce_1–Cu_4/ZSM-5 catalysts exposed to a flow of 500 ppm NH_3/Ar (50 mL min^{-1}) at 150 °C for different times.

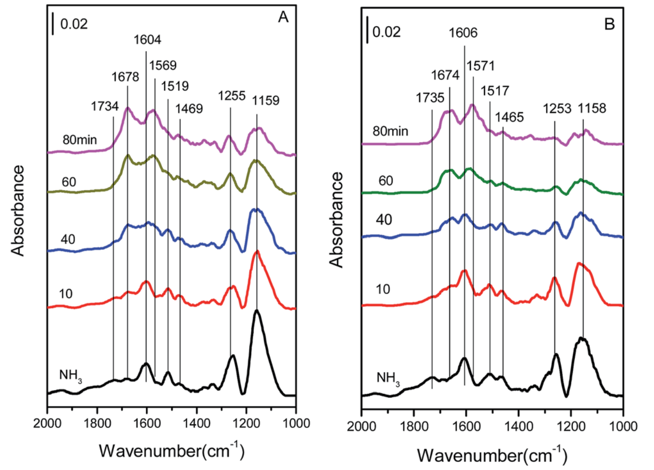

Fig. 12 *In situ* DRIFT spectra of (A) Cu_4/ZSM-5 and (B) Ce_1–Cu_4/ZSM-5 catalysts in the mixed gas of 500 ppm NO + 5 vol% O_2/Ar at different times, after adsorption of 500 ppm NH_3/Ar at 150 °C and blowing by Ar for 1 h.

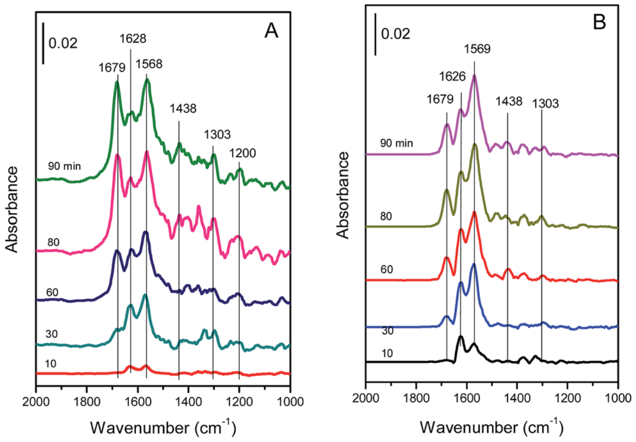

Fig. 13 *In situ* DRIFT spectra of the (A) Cu_4/ZSM-5 and (B) Ce_1–Cu_4/ZSM-5 catalysts exposed to a flow of 500 ppm NO + 5 vol% O_2/Ar (50 mL min^{-1}) at 150 °C for different times.

To study the reaction between NH_3 and adsorbed NO_x species, after the experiments of Fig. 13 were finished, the catalyst was purged with Ar (50 mL min^{-1}) for 1 h, and then was exposed to 500 ppm NH_3/Ar (50 mL min^{-1}). *In situ* DRIFT spectra of the catalyst were taken for different times and their results are presented in Fig. 14.

As shown in Fig. 14A, the intensities of the bands at 1568 cm^{-1} (assigned to bidentate nitrate) and 1628 cm^{-1} (assigned to bridged nitrate) decreased quickly with the increase of the exposure time in 500 ppm NH_3, indicating that bidentate and bridged nitrates are the reactive species with a high activity for the SCR reaction. On the contrast, the intensity of band at 1679 cm^{-1} (assigned to ionic nitrite species) was hardly changed even after NH_3 was passed over the catalyst for 80 min, showing that this species is inactive in SCR process. Simultaneously, the bands at 1159, 1255 and 1606 cm^{-1} originating from NH_3 adsorption species appear, and their intensities increase with the increase of the exposure time in NH_3.

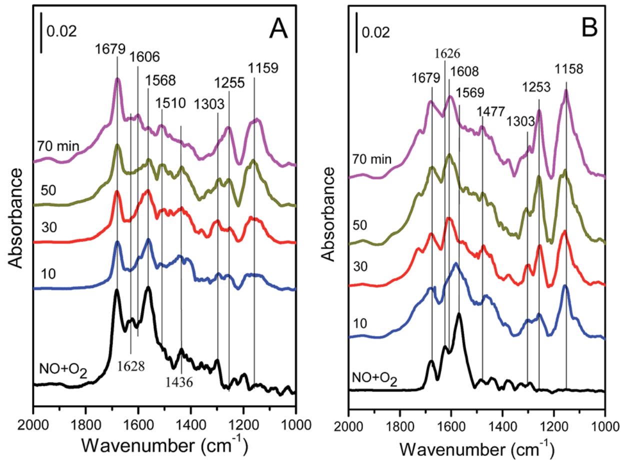

Fig. 14 *In situ* DRIFT spectra over (A) Cu_4/ZSM-5 and (B) Ce_1–Cu_4/ZSM-5 catalysts in 500 ppm NH_3/Ar for different times after adsorption of 500 ppm NO + 5 vol% O_2/Ar at 150 °C and blowing by Ar for 1 h.

Like the DRIFT results of the Cu_4/ZSM-5 catalyst, the intensities of the bands at 1569 cm^{-1} and 1626 cm^{-1} over the Ce_1–Cu_4/ZSM-5 catalyst decreased with the increase in the exposure time of NH_3, and these two bands disappeared after 30 min, which is less than that for the disappearance of these two bands over the Cu_4/ZSM-5 catalyst (60 min), indicating a high SCR activity of the Ce_1–Cu_4/ZSM-5 catalyst. On the contrary, the variation of the band at 1679 cm^{-1} was unobvious with the time. At the same time, the bands at 1158, 1253, 1477 and 1608 cm^{-1} originating from NH_3 adsorption species appeared, and their intensities increased with the increase of the exposure time in NH_3. Compared with the DRIFT results of the Cu_4/ZSM-5 catalyst, the intensities of the bands assigned to NH_3 adsorption species over the Ce_1–Cu_4/ZSM-5 catalyst are higher.

3.6.3 Proposed reaction pathway. As shown in Fig. 11, NH_3 mainly adsorbed on Lewis acid sites, as well as a little on Brønsted acid sites, and both NH_3 species adsorbed on Lewis acid sites and Brønsted acid sites are involved in the NH_3-SCR reaction. As a result, the bands corresponding to NH_3 adsorption in *in situ* DRIFT spectra (Fig. 12) decreased gradually when the catalysts pretreated with NH_3 are exposed to the mixed gas of NO and O_2.

For the Ce_1–Cu_4/ZSM-5 catalyst, the bands assigned to adsorbed NH_3 species on the Ce_1–Cu_4/ZSM-5 catalyst was decreased more quickly with the increase in the exposure time of NO + O_2 (Fig. 12B), indicating its higher SCR activity than the Cu_4/ZSM-5 catalyst. As shown in Fig. 13, the NO species can adsorb on the surface of the Cu_4/ZSM-5 and Ce_1–Cu_4/ZSM-5 catalysts in the forms of bridged and bidentate nitrates, ionic nitrite and nitrate, and bridged nitrite. The nitrite species tend to be oxidized to nitrate species over the Ce_1–Cu_4/ZSM-5 catalyst, because of its high catalytic activity for the oxidation reaction. When the catalysts pretreated with the mixed gas of NO and O_2 were exposed to NH_3, bidentate nitrate and bridged nitrate were consumed very quickly, while ionic nitrite species was hardly changed. These results indicate that bidentate nitrate and bridged nitrate over the Cu_4/ZSM-5 and Ce_1–Cu_4/ZSM-5 catalysts are the reactive species with a high SCR reactivity, and the SCR reaction is followed Langmuir–Hinshelwood mechanism over the Cu_4/ZSM-5 and Ce_1–Cu_4/ZSM-5 catalysts.

As above mentioned, when the catalysts pretreated with the mixed gas of NO and O_2 were exposed to NH_3, bidentate nitrate and bridged nitrate consumed very quickly and disappeared after 30 or 60 min (Fig. 14). However, when the catalysts pretreated with NH_3 were exposed to the mixed gas of NO and O_2, the bands corresponding to NH_3 adsorption in *in situ* DRIFT spectra (Fig. 12) decreased gradually, and a part of NH_3 species adsorbed on the catalysts surface remained still after 80 min. Therefore, when the catalysts pretreated with NH_3 were exposed to the mixed gas of NO and O_2, NO maybe adsorbed on the surface of catalysts pretreated with NH_3 firstly and then reacted with pre-adsorbed NH_3, resulting in the low reaction rate. Therefore, it can't be confirmed whether the SCR reaction over the Cu_4/ZSM-5 and Ce_1–Cu_4/ZSM-5 catalysts is followed Eley–Rideal mechanism.

3.7 Effect of SO_2 and H_2O on the SCR reaction

Fig. 15 shows the effect of SO_2 and H_2O on the catalytic activities of the Cu_4/ZSM-5 and Ce_1–Cu_4/ZSM-5 catalysts for the SCR reaction at 200 °C. Before adding H_2O or SO_2, NO_x conversion was 100% over the two catalysts and their activities was unchanged after 20 h of the reaction at 200 °C. When 2% H_2O was introduced into the feed gas, NO_x conversion over the Cu_4/ZSM-5 catalysts immediately decreased to 90.2% after 8 h of the reaction. After 2% H_2O in the feed gas was removed and lasting for 2 h, the NO_x conversion was returned to ~100%. After adding Ce in the Cu_4/ZSM-5 catalyst, its performance for H_2O resistance was improved, for instance, the NO_x conversion could hold ~94% in the presence of 2% water. And its NO_x conversion was returned to ~100% after removing 2% H_2O in the feed gas and lasting for 1.5 h. A similar trend can also be observed at high reaction temperature (450 °C) over the Cu_4/ZSM-5 and Ce_1–Cu_4/ZSM-5 catalysts (Fig. S2†).

When 50 ppm SO_2 was introduced into the feed gas, 100% NO_x conversion over the Cu_4/ZSM-5 catalysts was kept for 8 h and then decreased to 70.4% after the reaction of 6 h, but the deactivation of catalyst poisoned by SO_2 could not be recovered. However, it is obvious that the catalytic activity of the Ce_1–Cu_4/ZSM-5 catalyst was less affected by SO_2 than the Cu_4/ZSM-5 catalyst, that is to say, the Ce doping can improve the SO_2 resistance of the Cu_4/ZSM-5 catalyst. A similar trend can also be observed at high reaction temperature over the Cu_4/ZSM-5 and Ce_1–Cu_4/ZSM-5 catalysts (Fig. S2†). It is well known that the ammonium sulfate and copper sulfate deposited on the catalyst surface can cover available active sites and block zeolite channels,[46] and they could not be decomposed and removed at 200 °C on the catalyst surface,[47] resulting in a deactivation of catalyst. The presence of Ce in the Cu_4/ZSM-5 catalyst can make SO_2 firstly deposit on the Ce site to form a stable Ce sulfate, which can inhibit the formation of ammonium sulfate and copper sulfate on the catalyst surface in the SCR process, improving the excellent sulfur tolerance of the Ce_1–Cu_4/ZSM-5 catalyst.

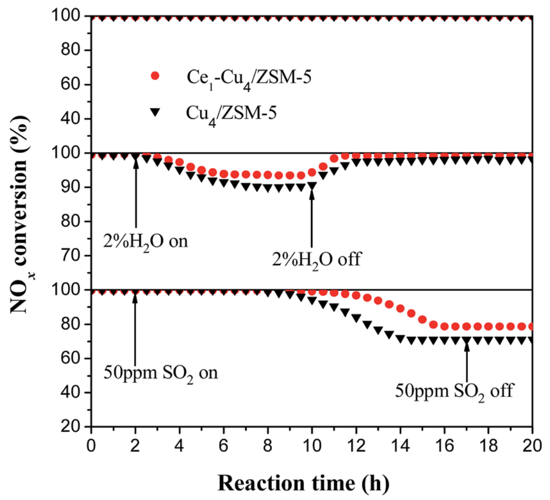

Fig. 15 Effect of SO_2 and H_2O on the catalytic activities of Cu_4/ZSM-5 and Ce_1–Cu_4/ZSM-5 catalysts for SCR reaction at 200 °C. (Reaction conditions: 0.2 g catalyst, 500 ppm NO, 500 ppm NH_3, 5% O_2, Ar to balance, GHSV = 55 000 h^{-1}).

4. Conclusions

In summary, the addition of Ce can markedly improve the catalytic activity of the Cu/ZSM-5 catalyst for NH_3-SCR reaction and enhance its SO_2 and water resistance. Adding Ce in the Cu_4/ZSM-5 catalyst promoted the enrichment of copper species on the catalyst surface and increased the surface concentrations of both isolated Cu^{2+} ions and CuO crystallites, resulting in the improvement of the redox properties and the NO adsorption ability of the Cu_4/ZSM-5 catalyst. The Ce amount would affect the catalytic performance of Ce_x–Cu/ZSM-5, especially the NH_3-SCR activity at high temperature. When the Ce_1–Cu_4/ZSM-5 catalyst (Ce/Cu = 1/4, wt) was used, the temperature window for more than 90% NO_x conversion was extended to 185–470 °C, which broadened the operation window about 45 °C, because more nitrite and nitrate species on the Ce_1–Cu_4/ZSM-5 catalyst surface can participate the SCR reaction than that on the surface of the Cu_4/ZSM-5 catalyst, and the Ce-doping sample can adsorb NO at lower temperature. *In situ* DRIFTS results indicated that the Langmuir–Hinshelwood mechanism for the NH_3-SCR reaction over the Cu_4/ZSM-5 and Ce_1–Cu_4/ZSM-5 catalysts was confirmed, but Eley–Rideal mechanism can't be sure yet.

Acknowledgements

This work was supported financially by the National Natural Science Foundation of China (21577034, 21333003), the Commission of Science and Technology of Shanghai Municipality (15DZ1205305) and the Fundamental Research Funds for the Central Universities (WJ1514020).

Notes and references

1 A. Brückner, F. Hipler, G. Auer, E. Löffler and W. Grünert, *J. Catal.*, 2012, **286**, 237.
2 Z. M. Liu, J. H. Li and S. I. Woo, *Energy Environ. Sci.*, 2012, **5**, 8799.
3 W. P. Shan, F. D. Liu, H. He, X. Y. Shi and C. B. Zhang, *Catal. Today*, 2012, **184**, 160.
4 M. J. Li, Y. Yeom, E. Weitz and W. M. H. Sachtler, *J. Catal.*, 2005, **235**, 201.
5 X. F. Yang, Z. L. Wu, M. Moses-Debusk, D. R. Mullins, S. M. Mahurin, R. A. Geiger, M. Kidder and C. K. Narula, *J. Phys. Chem. C*, 2012, **116**, 23322.
6 H. Sjövall, L. Olsson, E. Fridell and R. J. Blint, *Appl. Catal., B*, 2006, **64**, 180.
7 G. Carja, Y. Kameshima, K. Okada and C. D. Madhusoodana, *Appl. Catal., B*, 2007, **73**, 60.
8 J. L. de Lucas, F. Valverde, A. Dorado and I. Romero, *J. Mol. Catal. A: Chem.*, 2005, **225**, 47.
9 J. H. Park, H. J. Park, J. H. Baik, I. S. Nam, C. H. Shin, J. H. Lee, B. K. Cho and S. H. Oh, *J. Catal.*, 2006, **240**, 47.
10 X. F. Tang, Y. G. Li, X. M. Huang, Y. D. Xu, H. Q. Zhu, J. G. Wang and W. J. Shen, *Appl. Catal., B*, 2006, **62**, 265.

11 G. Carja, Y. Kameshima, K. Okada and C. D. Madhusoodana, *Appl. Catal., B*, 2007, **73**, 60.

12 Z. B. Wu, R. B. Jin, Y. Liu and H. Q. Wang, *Catal. Commun.*, 2008, **9**, 2217.

13 S. M. Lee, K. H. Park and S. C. Hong, *Chem. Eng. J.*, 2012, **195–196**, 323.

14 K. Liu, F. D. Liu, L. J. Xie, W. P. Shan and H. He, *Catal. Sci. Technol.*, 2015, **5**, 2290.

15 Y. P. Zhang and M. Flytzani-Stephanopoulos, *J. Catal.*, 1996, **164**, 131.

16 J. Y. Yan, W. M. H. Sachtler and H. H. Kung, *Catal. Today*, 1997, **33**, 279.

17 L. Pang, C. Fan, L. N. Shao and K. P. Song, *Chem. Eng. J.*, 2014, **253**, 394.

18 B. J. Dou, G. Lv, C. Wang, Q. Hao and K. Hui, *Chem. Eng. J.*, 2015, **270**, 549.

19 F. Bin, *Appl. Catal., B*, 2014, **150–151**, 532.

20 B. Pereda-Ayo, U. D. L. Torre, M. J. Illán-Gómez, A. Bueno-López and J. R. González-Velasco, *Appl. Catal., B*, 2014, **147**, 420.

21 L. Wang, J. R. Gaudet, W. Li and D. Weng, *J. Catal.*, 2013, **306**, 68.

22 M. H. Groothaet, J. A. van Bokhoven, A. A. Battiston, B. M. Weckhuysen and R. A. Schoonheydt, *J. Am. Chem. Soc.*, 2003, **125**, 7629.

23 T. Zhang, J. Liu, D. Wang, Z. Zhao, Y. Wei, K. Cheng, G. Jiang and A. Duan, *Appl. Catal., B*, 2014, **148–149**, 520.

24 S. Yashnik and Z. Ismagilov, *Appl. Catal., B*, 2015, **170–171**, 241.

25 Y. Fu, W. Zhan, Y. Guo, Y. Wang, X. Liu, Y. Guo, Y. Wang and G. Lu, *Microporous Mesoporous Mater.*, 2015, **214**, 101.

26 T. Zhang, J. Liu, D. X. Wang, Z. Zhao, Y. C. Wei, K. Cheng, G. Y. Jiang and A. J. Duan, *Appl. Catal., B*, 2014, **148–149**, 520.

27 G. H. Kuehl and H. K. C. Timken, *Microporous Mesoporous Mater.*, 2000, **35–36**, 521.

28 L. J. Lobree, I. C. Hwang and J. A. Reimer, *J. Catal.*, 1999, **186**, 242–253.

29 X. Liang, J. X. Li, Q. C. Lin and K. Q. Sun, *Catal. Commun.*, 2007, **8**, 1901.

30 X. D. Wu, F. Lin, H. B. Xu and D. Weng, *Appl. Catal., B*, 2010, **96**, 101.

31 A. de Lucas, J. L. Valverde, F. Dorado, A. Romero and I. Asencio, *J. Mol. Catal. A: Chem.*, 2005, **225**, 47.

32 J. Chen, M. Shen, X. Wang, G. Qi, J. Wang and W. Li, *Appl. Catal., B*, 2013, **251**, 134.

33 L. Wang, W. Li, S. J. Schmieg and D. Weng, *J. Catal.*, 2015, **324**, 98.

34 F. Gao, J. H. Kwak, J. Szanyi and C. H. F. Peden, *Top. Catal.*, 2013, **56**, 1441.

35 H. Y. Zhu, J. H. Kwak, C. H. F. Peden and J. Szanyi, *Catal. Today*, 2013, **205**, 16.

36 L. Wang, W. Li, G. S. Qi and D. Weng, *J. Catal.*, 2012, **289**, 21.

37 W. S. Kijlstra, D. S. Brands, H. I. Smit, E. K Poels and A. Bliek, *J. Catal.*, 1997, **171**, 219.

38 S. Brandenberger, O. Kröcher, A. Wokaun, A. Tissler and R. Althoff, *J. Catal.*, 2009, **268**, 297.

39 W. Shan, F. Liu, H. He, X. Shi and C. Zhang, *Appl. Catal., B*, 2012, **115–116**, 100.

40 S. Liu, X. D. Wu, D. Weng and R. Rani, *Ind. Eng. Chem. Res.*, 2012, **51**, 2271.

41 R. D. Zhang, W. Yang, N. Luo, P. X. Li, Z. G. Lei and B. H. Chen, *Appl. Catal., B*, 2014, **146**, 94.

42 J. Szanyi, J. H. Kwak, H. Y. Zhu and C. H. F. Peden, *Phys. Chem. Chem. Phys.*, 2013, **15**, 2368.

43 K. Hadjiivanov, A. Penkova, M. Daturi, J. Saussey and J. C. Lavalley, *Chem. Phys. Lett.*, 2003, **377**, 642.

44 K. I. Hadjiivanova, *Catal. Rev.: Sci. Eng.*, 2000, **42**, 71.

45 I. Atribak, B. Azambre, A. Bueno López and A. García-García, *Appl. Catal., B*, 2009, **92**, 126.

46 Z. X. Ma, H. S. Yang, F. Liu and X. B. Zhang, *Appl. Catal., A*, 2013, **467**, 450.

47 J. Yu, F. Guo, Y. L. Wang, J. H. Zhu, Y. Y. Liu and F. B. Su, *Appl. Catal., B*, 2010, **95**, 160.